Desalination and Water Treatment
www.deswater.com
doi: 10.1080/19443994.2014.934726

56 (2015) 274–283
September

Taylor & Francis
Taylor & Francis Group

Adsorption of sulfate from natural water on calcined Mg–Fe layered double hydroxides

Jiming Liu, Xiuping Yue*, Yang Yu, Yu Guo

College of Enviromental Science and Technology, Taiyuan University of Technology, Shanxi, China, Tel. +86 351 6010243; email: liujiming@tyut.edu.cn (J. Liu), Tel. +86 351 6010243; Fax: +86 351 6010214; email: yuexiuping@tyut.edu.cn (X. Yue), Tel. +86 351 6010243; emails: tyut2002489@126.com (Y. Yu), 676618568@qq.com (Y. Guo)

Received 5 December 2013; Accepted 6 June 2014

ABSTRACT

The calcined Mg–Fe layered double hydroxides (Mg–Fe–CLDHs) with the Mg–Fe molar ratio of 3 were used as adsorbents to remove sulfate in natural water. The Mg–Fe–CLDHs were synthesized by the co-precipitation method. The influences of initial adsorbent concentration, temperature, and pH on the adsorption of sulfate on Mg–Fe–CLDHs were evaluated. Three kinetic models and two isotherms were used to fit the experimental data, and it was found that the pseudo-second order kinetics model and Langmuir isotherm model could be used to describe the uptake process appropriately. Characteristics of the adsorbents and adsorption mechanism were analyzed by XRD, FT-IR, BET, TG-DSC, and SEM.

Keywords: Layered double hydroxides; Calcined; Sulfate removal; Adsorption; Natural water; Equilibrium; Kinetic

1. Introduction

Sulfate is naturally present in the water systems. It mainly originates from the dissolution of numerous sulfate minerals and the drainage of industrial effluent containing sulfate components. Sulfate in natural water can produce noticeable taste and the high levels of sulfate may cause a laxative effect in unaccustomed consumers. It is generally considered that taste impairment of sulfate level below 250 mg/L is minimal [1]. Several methods have been used to remove sulfate from water, including adsorption [2,3], precipitation [4,5], separation [6,7], electrochemistry [7,8] and ion exchange [9]. In these methods, adsorption is one of the promising methods to remove sulfate in water. Therefore, it is necessary to develop an ideal adsorbent to meet water treatment requirement.

Layered double hydroxides (LDHs), also known as hydrotalcite-like compounds or anionic clay, are a class of materials usually applied to remove anions due to their large surface area, high anion exchange capacity, thermal stability, and convenient synthesization. The general formula is $[M^{2+}_{1-x}M^{3+}_{x}(OH)_2]^{x+}(A^{n-})_{x/n}\cdot mH_2O$, where M^{2+} (Mg^{2+}, Zn^{2+}, Ni^{2+}, Cu^{2+}, etc.) and M^{3+} (Al^{3+}, Mn^{3+}, Cr^{3+}, Fe^{3+}, etc.) are metal cations that occupy octahedral sites in the hydroxide layers. A^{n-} is an exchangeable anion (CO_3^{2-}, NO_3^-, Cl^-, etc.), located in the interlayer space between two brucite sheets; x is the ratio of $M^{3+}/(M^{2+}+M^{3+})$; the layer charge depends on the M^{2+}/M^{3+} ratio [10]. LDHs calcined within a certain temperature range exhibit a striking property, the so-called "memory effect" [11] that at a relatively low calcination temperature, the calcined products can

*Corresponding author.

easily reconstruct the original layered structure in an aquatic environment. In these calcined Mg–Fe LDHs (hereafter as Mg–Fe–CLDHs) are receiving greater interests in the environmental community and have been evaluated as adsorbents for the removal of selenite, phosphate, acid brown 14 dye, perchlorate, arsenate and fluoride [12–17].

For Mg–Fe–CLDHs exhibits remarkable properties for the removal of anion from aqueous solutions, it would be of interest to combine the anion adsorption properties of Mg–Fe–CLDHs with the anions of sulfate. In this present work, Mg–Fe–CLDHs were used as adsorbents to remove sulfate in natural water. Various adsorption parameters such as pH, adsorbent dose, temperature, etc. were investigated. In addition, the adsorption isotherms, kinetic models and adsorption mechanism were studied in detail.

2. Experimental

2.1. Reagents

$Mg(NO_3)_2{\cdot}6H_2O$, $Fe(NO_3)_3{\cdot}9H_2O$, NaOH and Na_2CO_3 used in this study were of analytical grade (AR). All the water utilized was deionized water. The required sulfate-enriched natural water was obtained from Xiangfeng Supply Water Plant in Shanxi, China in March 2013. Its contents were listed in Table 1.

2.2. Preparation of adsorbents

Layered double hydroxides (LDHs) were prepared by the co-precipitation method [18]. A solution of 100 mL containing 1.50 mol of $Mg(NO_3)_2{\cdot}6H_2O$ and 0.50 mol of $Fe(NO_3)_3{\cdot}9H_2O$ (Mg–Fe molar ratio 3:1) as well as a mixed solution of 2.00 M NaOH and 0.5 M Na_2CO_3 was added into 300 mL of deionized water in drops at the same time under vigorously stirring and the pH was maintained at about 10. The suspension was aged 24 h at 65℃ for crystallization. Subsequently, the resulting material was separated by vacuum filtration and washed thoroughly with deionized water till the washings were neutral, and the filter cake was dried at 80℃ for 12 h. The Mg–Fe–CLDHs was obtained by heating Mg–Fe LDHs in a muffle furnace at 400℃ for 4 h.

Table 1
Chemical composition and characteristics of the natural water

Parameters	Values	Parameters	Values
pH	6.8	Cl^-/(mg/L)	75.7
TDS/(mg/L)	635	SO_4^{2-}/(mg/L)	598.6
Fe^{3+}/(mg/L)	0.04	F^-/(mg/L)	0.9
Turbidity/NTU	0.7	NO_3^-(N)/(mg/L)	0.7
Mn^{2+}/(mg/L)	<0.1	Chromaticity	0.5
Cu^{2+}/(mg/L)	<0.1	Zn^{2+}/(mg/L)	<0.05

2.3. Characterization of adsorbents

The X-ray powder diffraction pattern (XRD) of the samples was obtained in Shimadzu-XRD-6000 (Japan) with an auto-divergent slit fitted with a graphite monochromator using Cu Kα radiation at 40 kV and 30 mA. The scanning scope is 5˚–70˚ every 0.02˚ (2θ) at a scanning speed of 8 min^{-1}. The fourier transform infrared (FT-IR) of the samples were recorded at room temperature according to the KBr (Sigma-Aldrich ≥99%) pellet method (sample: KBr = 1:100) on a PerkinElmer Spectrum 100 spectrophotometer in the 400–4,000 cm^{-1} range with the average of 50 scans. The resolution was better than 4 cm^{-1}. The thermogravimetric analysis and differential scanning calorimetry (TG-DSC) analysis data were obtained with a thermal analyzer (NETZSCH STA 409PC/PG, Germany) in the temperature range of 40–600℃ with the heating rate of 30 K/min in N_2 flow (40 mL/min). The specific surface areas of adsorbents were determined by the Brunner–Emmett–Teller (BET) method in a ASAP 2020 (USA) with N_2 gas. The samples were evacuated overnight at 90℃. Morphology of the samples was examined by scanning electron microscope (SEM) (JEOL JSM-6300 Scanning Microscope, Japan). The contents of Mg and Fe in LDHs were determined by Inductively Coupled Plasma-Atom Emission Spectrum (ICP-AES, optima2000, USA). The carbon content and nitrogen element of the samples were analyzed by Element analysis method (PE series 2 CHNS/O 2400, USA).

2.4. Adsorption experiments

The adsorption of sulfate was studied at 30 ± 1℃ in the batch test. The Mg–Fe–CLDHs (0.37 g) was added into 50 mL natural water in a 150 mL conical flask. After continuous vibration at 180 rpm for 4-h in a thermostat, the solid material was separated by filtration. The sulfate concentration was determined spectrophotometrically at 420 nm. A number of parameters, such as adsorbent dose, pH, contact time and temperature, have been changed largely in order to understand the adsorption characteristics. Adsorption isotherms were obtained by mixing an initial dosage range of Mg–Fe–CLDHs (0.27–0.41 g) with 50 mL of natural water at 30 ± 1℃ and testing the

equilibrium sulfate concentrations after 4-h contact. Kinetics of sulfate adsorption was investigated with the 0.37 g Mg–Fe–CLDHs as the adsorbents being added into 50 mL of natural water and the soluble sulfate concentration variation with different adsorption time being monitored.

The adsorption amount of sulfate on Mg–Fe–CLDHs was calculated according to the following equation:

$$q_e = \frac{(C_0 - C_e)V}{W} \quad (1)$$

where q_e is the equilibrium concentration of sulfate adsorbed on Mg–Fe–CLDHs; V is the volume of solution (L); C_0 (mg/L) and C_e (mg/L) are the initial concentration and the equilibrium concentration of SO_4^{2-}, respectively; W is the mass of adsorbent (g).

3. Results and discussion

3.1. Characteristics of LDHs

The chemical analysis by ICP-AES showed that the determined M^{2+}/M^{3+} ratio was 2.78:1, which was similar to the nominal ratio used in the synthesis mixture, indicating an efficient co-precipitation. Combined with the element analysis and the TG curve of Mg–Fe LDHs, the chemical formula of Mg–Fe LDHs was determined to be $Mg_{0.76}Fe_{0.24}(OH)_2(CO_3)_{0.23}(NO_3)_{0.01}(0.56H_2O)$.

Representative XRD patterns of the LDH materials are shown in Fig. 1. The XRD pattern of Mg–Fe LDH samples shows sharp and symmetric peaks, which indicate that the samples are well crystallized, and peak corresponding to (003), (006), (110), the characteristic reflections of the hydrotalcite structure (Fig. 1(a)). For the samples calcined at 400 ℃, the (003) and (006) reflections (peaks) disappeared, indicating that hydrotalcite structure was largely destroyed and the stacking of the layers was disordered. Only the diffused peaks corresponding to MgO are observed (Fig. 1(b)).

FT-IR study of Mg–Fe LDHs calcined at 400 ℃ and Mg–Fe–CLDHs after adsorption were carried out in order to confirm the presence of various groups. FT-IR spectrum of Mg–Fe LDH is presented in Fig. 2(a). The broad bands in the region between 3,400 and 3,700 cm^{-1} can be assigned to −OH stretching vibrations of hydroxyl groups in the brucite layers and interlayer water molecules [19]. The peak at 1,650 cm^{-1} can be assigned to the adsorbed interlayer water. The band at 1,359 cm^{-1} is assigned to the vibration of carbonate ions and nitrate ions [20]. The band below 1,000 cm^{-1} is assigned to the metal bands [21]. According to FT-IR spectrum of Mg–Fe–CLDHs (Fig. 2(b)), the well-defined diffraction peaks of the parent samples are replaced by broad peaks, indicating the nanocrystalline material with very small nanoparticles or even an amorphous phase. The band of 1,359 cm^{-1} disappeared, indicating that carbonate ions were evaporated.

According to TG and DSC analysis of LDHs (Fig. 3), the thermal decomposition clearly consists of two distinct steps. The first step below 200 ℃ can be attributed to the dissipation of interlayer water, with one corresponding endothermic peak (182.1 ℃) in the DSC curve. The corresponding mass loss was found to be 10%. The second step between 200 and 500 ℃ was related to dissipation of hydroxyl groups in the brucite layer and interlayer CO_3^{2-} anions, with a corresponding endothemic peak (358 ℃) in the DSC

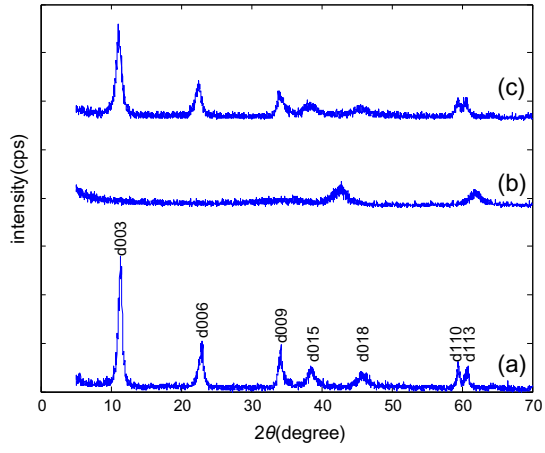

Fig. 1. XRD pattern of Mg–Fe LDHs, calcined at 400 ℃ and Mg–Fe–CLDHs after adsorption.

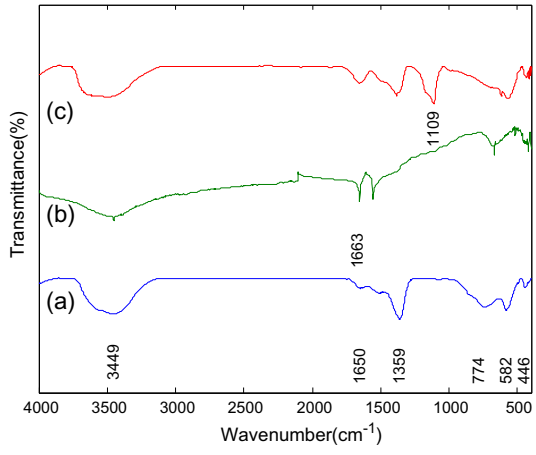

Fig. 2. FTIR pattern of Mg–Fe LDHs, calcined at 400 ℃ and Mg–Fe–CLDHs after adsorption.

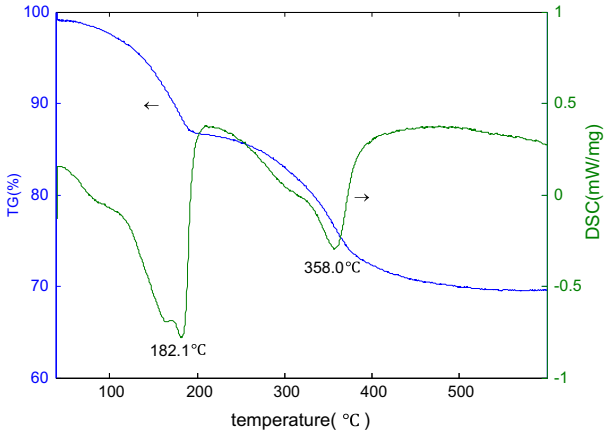

Fig. 3. TG-DSC pattern of Mg–Fe LDHs.

curve. The corresponding mass loss was found to be 16%. The TG-DSC shown for the Mg–Fe–LDHs are the typical results reported for LDHs [3,22].

SEM of Mg–Fe LDHs before and after being calcined at 400℃ (Fig. 4) was obtained. The Mg–Fe LDH adsorbents in Fig. 4(a) showed the characteristics of plate-like morphology and hexagonal crystallite. Upon calcination, the Mg–Fe–CLDH samples sintering occurred. As shown in Fig. 4(b), the particles are formed by the aggregation of very small platy crystallites.

The N_2 adsorption-desorption isotherms of representative Mg–Fe LDH samples are shown in Fig. 5. The insert shows the pore size distribution determined by the Barrett–Joyner–Halenda (BJH) analysis using the adsorption data. The adsorption isotherms of the samples exhibit the characteristics of the type II isotherms (according to IUPAC classification), which is usually associated with non-porous or macroporous materials and represents unrestricted monolayer-multilayer adsorption [23]. Furthermore, the isotherms of the LDH samples exhibit clear hysteresis loops, which resemble type H3 loops (IUPAC classification) related to slit-shaped pore or voids created within aggregates of platy particles. The pore size distributions of the samples are broad and the average pore diameter increases significantly (about >100 nm), which is also verified by the corresponding pore size distribution of the samples.

The pore size distribution of the samples was determined by the BJH method from the desorption branch of the isotherms (Table 2). It can be seen that the sample of Mg–Fe LDHs exhibits the high specific surface area (65 m^2/g) as well as the high total pore volume (0.53 cm^3/g). While Mg–Fe–CLDH samples, The BET surface area and the pore volume were as higher as 74 m^2/g and 0.64 cm^3/g, respectively, which was probably caused by the formation of amorphous phase of magnesium iron mixed oxides and the aggregation of the layered structure.

3.2. Removal of sulfates with the CLDH adsorbents

3.2.1. Dosage effect of adsorbents

The variation of the dosage of adsorbents was performed using the ratio of 0.27–0.41 g. The as-synthesized Mg–Fe–CLDHs were stirred for 4 h. The dosage effect of adsorbent on the loading capacity of CLDH adsorbents is shown in Fig. 6. As shown in Fig. 6, the dosage of CLDH adsorbents significantly influenced the removal efficiency of sulfate. The loading capacity increased with the increment of the adsorbent dosage. When the sulfate solution was treated with 7.4 g/L Mg–Fe–CLDHs, the removal percentage of sulfate reached 77% ± 1.7, indicating about 140 g/L residual sulfate concentration in the solution, which was far below the WHO standard. Therefore, the dosage amount is selected as 7.4 g/L for further investigation. The results suggested that the CLDH adsorbent is a

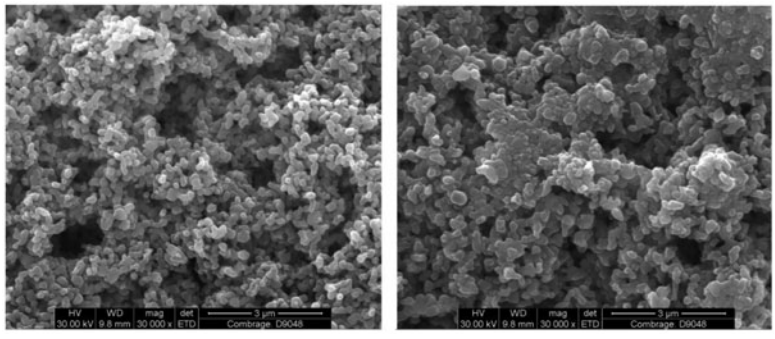

Fig. 4. SEM images of Mg–Fe LDHs, calcined at 400℃.

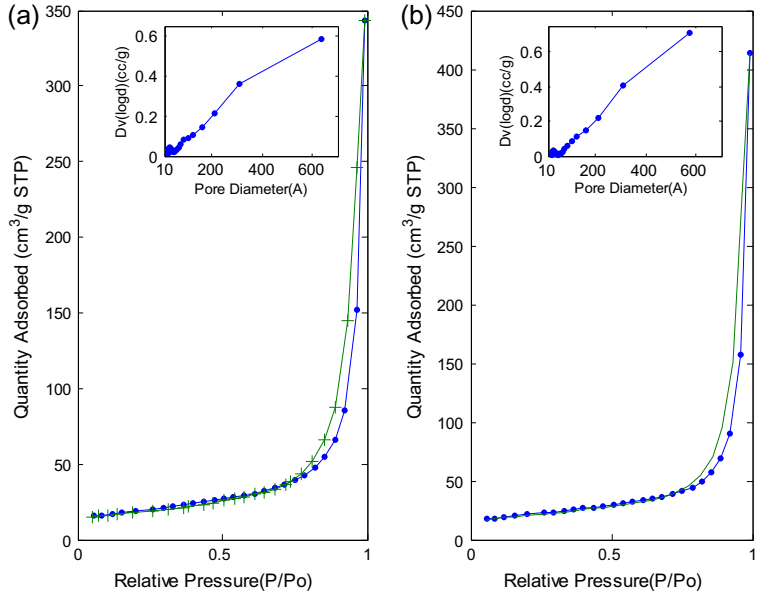

Fig. 5. N_2 adsorption-desorption isotherms and pore size distribution based on BJH analysis of adsorption data (inert) for representative LDH samples: (a) Mg–Fe LDHs; (b) Mg–Fe–CLDHs.

Table 2
Surface area and pore properties of the Mg–Fe LDHs and Mg–Fe–CLDHs

CLDHs	Surface area (SBET) (m^2/g)	Pore volume (cm^3/g)	Average pore width (nm)
Mg–Fe LDHs	65	0.53	307
Mg–Fe–CLDHs	74	0.64	349

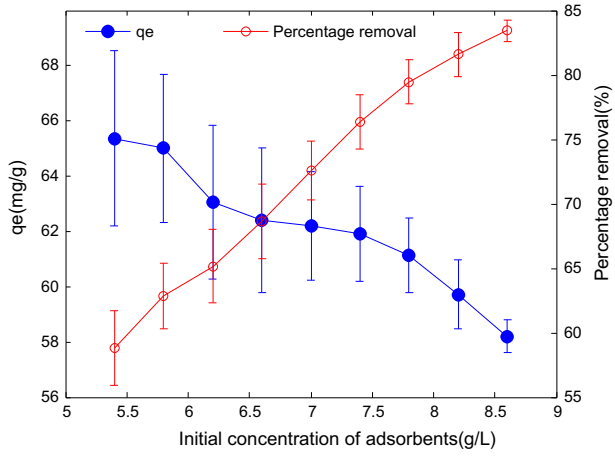

Fig. 6. Effect of initial concentration of Mg–Fe–CLDHs on sulfate adsorption.

potential efficient adsorbent for the treatment of natural water with high concentration of anionic sulfate.

3.2.2. Temperature effect on sulfate uptake

Temperature variation is one of the most important parameter in the adsorption process. A series of experiments at 20, 30, 40, and 50°C were investigated to study the effect of temperature. According to the influence of temperature on the adsorption of sulfate (Fig. 7), the equilibrium concentration of sulfate decreased with the rising temperature and the adsorption ratio increased from 68 to 90%, indicating that the interaction of adsorbate and adsorbent is endothermic in nature. In addition, the equilibrium pH values were very close, almost all of 11, suggesting that the temperature change has no effect on the equilibrium pHs.

3.2.3. Effect of pH on sulfate uptake

In order to give the more detailed information about the adsorption mechanism, the effect of pH on sulfate adsorption at 30°C were investigated. As shown in Fig. 8, when the solution pH was increased from 3.0 to 11.0, the adsorption capacity of sulfate

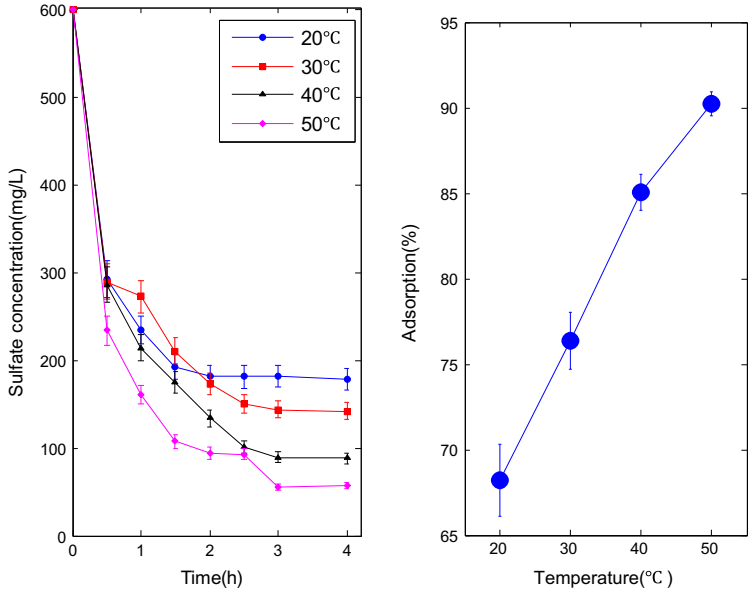

Fig. 7. Effect of temperature of Mg–Fe–CLDHs on sulfate adsorption.

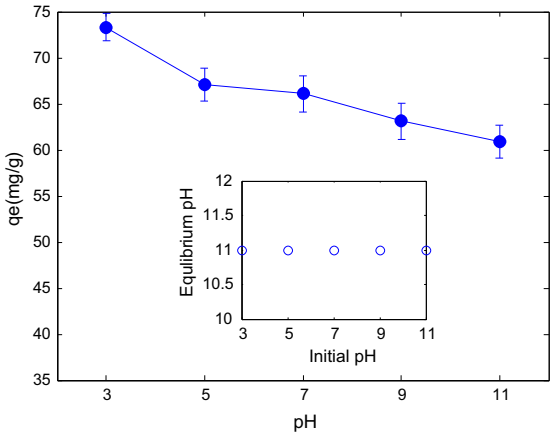

Fig. 8. Effect of initial pH solution on sulfate adsorption by Mg–Fe–CLDHs.

onto the samples decreased gradually. The adsorption capacity at pH 3 was the highest, which is related to electrostatic attraction and ion exchange interaction. However, even at alkaline condition, pH was higher than pH_{PZC} of the Mg–Fe–CLDH adsorbents (around 7.0 [13]), the adsorption capacity was still kept a comparably high value. It indicated that the effect of initial pH over a wide pH range on the adsorption of SO_4^{2-} was negligible. The possible reason is the reconstruction of the LDH structure with the intercalation of sulfate into the CLDH in aqueous solutions.

Moreover, an examination of the equilibrium solution pH values for sulfate after adsorption was also carried out. The equilibrium pH kept stable at 11 throughout the initial pH range, indicating that ions exchange interaction existed between anions and hydroxyl ions in the adsorption process.

3.2.4. Adsorption isotherm analysis

The isotherm models of Langmuir and Freundlich were investigated to determine the experimental adsorption equilibrium data of sulfate on CLDH adsorbents. These models are represented mathematically [24].

The non-linearized and linearized form of Langmuir isotherm can be described as the following equations:

$$q_e = \frac{q_m K_L C_e}{1 + K_L C_e} \tag{2}$$

$$\frac{C_e}{q_e} = \frac{C_e}{q_m} + \frac{1}{K_L q_m} \tag{3}$$

where C_e is the equilibrium concentration of the anions in natural water; q_e is equilibrium adsorption capacity (mg/g); q_m is the theoretical saturated adsorption capacity (mg/g); K_L is the Langmuir adsorption constant related to the energy of adsorption (L/mg).

The non-linearized and linearized form of Freundlich isotherm can be described as the following equations:

$$q_e = K_F C_e^{1/n} \tag{4}$$

$$\ln q_e = \ln K_F + \frac{1}{n} \ln C_e \tag{5}$$

where K_F is the Freundlich constant; $1/n$ is the heterogeneity factor.

The root mean square error (RMSE) for the straight line fit of each model was calculated as following equations [25]:

$$\text{RMSE} = \left[\sum (q_t - q_t^*)^2/(n-m)\right]^{0.5} \tag{6}$$

Where q_t and q_t* are the amount of sulfate adsorbed (mg/g) at time t, obtained from the laboratory experiments and predicted by the models, respectively. The n value is the number of measurements and the m value is the number of fitted parameters.

The results of fitting Freundlich and Langmuir equations to isotherm curves are summarized in Fig. 9 and Table 3. The higher values of Regression coefficients (R^2) and lower values of RMSE showed that the adsorption data were better fit to the Langmuir isotherm model, indicating that the adsorption process might be a chemical adsorption and that anions might be adsorbed in the formation of monolayer coverage on the adsorbent surface [13]. It can be seen that the maximum adsorption capacity is calculated to be 68.7 mg/g, which is greater than those of reported for activated carbon developed from coconut coir pith (4.9 mg/g) [3] and raw straw (11.68 mg/g) [9]. The positive K_L value indicates that adsorption system is favorable.

3.2.5. Adsorption kinetic studies

Adsorption kinetics is one of the most important characteristics which represent the adsorption efficiency. The adsorption rate of sulfate adsorption was tested with the CLDH samples to determine the time required for adsorption equilibrium. Three kinetic order models were studied to fit the experimental data: the pseudo-first-order, the pseudo-second-order, and the intraparticle diffusion model.

The pseudo-first order model can be expressed in integrated form as follows [26]:

$$\ln(q_e - q_t) = \ln(q_e) - k_1 t \tag{7}$$

where q_e and q_t are the adsorption capacity of the adsorbate (mg/g) at equilibrium and at time (min), respectively; k_1 is the rate constant of adsorption (min^{-1}), which can be calculated from the plot of $\ln(q_e - q_t)$ against t.

The pseudo-second order model can be expressed as follows [27]:

$$\frac{t}{q_t} = \frac{1}{k_2 q_e^2} + \frac{t}{q_e} \tag{8}$$

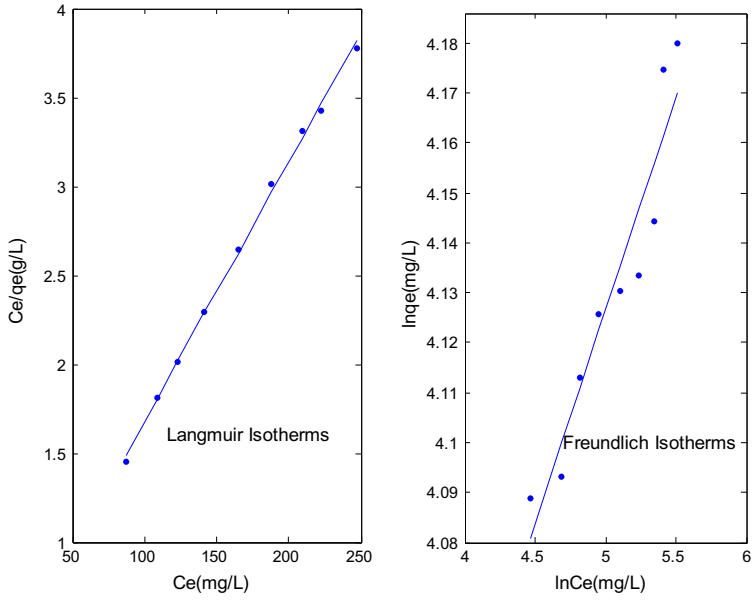

Fig. 9. Isotherms of sulfate adsorption onto the calcined Mg–Fe LDH from natural water.

Table 3
Langmuir and Freundlich isotherm constants of sulfate adsorption onto CLDH

Freundlich constants				Langmuir constants			
K_F	n	R^2	RMSE	Q_{max} (mg/g)	K_L (L/mg)	R^2	RMSE
.45	11.29	0.953	0.089	68.73	0.064	0.999	0.030

where k_2 represents the rate constant of pseudo-second order adsorption (g/(mg min)); the q_e as well as k_2 can be obtained from the linear plot of t/q_t against t.

The intraparticle diffusion model can be obtained with Weber-Morris equation as follows [28]:

$$q_t = K_F t^{1/2} + C$$

where K_F is the intraparticle diffusion rate constant (mg/(g $min^{0.5}$)).

The results were shown in Fig. 10 and Table 4. The sulfate adsorption by the CLDH followed pseudo-second order kinetics the best with high correlation coefficients ($R^2 > 0.99$) and low RMSE. The calculated sulfate adsorption capacity at equilibrium is 69 mg/g, which is consistent with the tested values. The low values of k_2 indicated that the rates of sulfate adsorption process were fast. These results show that the pseudo-second-order sorption mechanism is dominant and that the overall rate constant of sorption process appears to be controlled by a chemisorption process.

As for the intraparticle diffusion model results from Fig. 10(d), the plot obtained for each concentration consists of three straight linear segments, indicating that three steps occur in the adsorption processes. The first stage ($t^{1/2} < 1.4$) is attributed to the sulfate anions diffusion from liquid phase to adsorbent external surface, while the second stage ($1.4 < t^{1/2} < 1.58$) is attributed to the gradual adsorption stage. The intraparticle diffusion is rate-controlled. The third stage ($t^{1/2} > 1.58$) is that the adsorption process of sulfate anions reaches its equilibrium stage, corresponding to a chemical reaction. Such a multiple nature for the relationship confirms that the adsorption of sulfate anions on CLDHs appeared to be a complex process.

3.3. Proposed adsorption mechanism

The adsorption mechanism was determined by XRD and FT-IR analysis. According to the XRD patterns after the adsorption of sulfate (Fig. 1(c)), upon the treatment of the Mg–Fe–CLDHs with sulfate

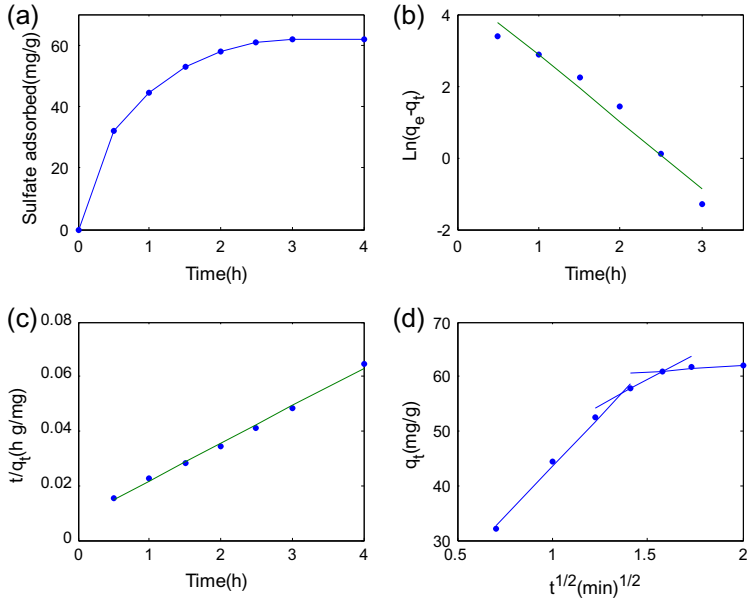

Fig. 10. Kinetics of the sulfate adsorption on the Mg–Fe–CLDHs from: (a) natural water, the data fitting by, (b) pseudo-first-order, (c) pseudo-second-order, and (d) intraparticle diffusion models.

Table 4
Kinetic models for sulfate adsorption on Mg–Fe–CLDHs from natural water and the calculated constants

Kinetic models	Parameter			
Pseudo-first-order	k_1 (min^{-1})	q_e (mg/g)	R^2	RMSE
	0.066	80.6	0.964	0.325
Pseudo-second-order	K_2 (g/(mg min))	q_e (mg/g)	R^2	RMSE
	0.0002	68.7	0.998	0.001
Intraparticle diffusion	K_F (mg/(g $min^{0.5}$))	R^2	RMSE	
	2.44	0.935	3.9695	

solution, partial reconstruction of original structure of the material was found and it was consistent with the results in previous structural studies of LDHs. However, the peaks, particularly (003) and (006), were broadened and the intensity of the peaks decreased compared with those of the original LDHs, indicating some reductions in crystallinity after calcinations and rehydration.

According to the FT-IR spectra of the Mg–Fe–CLDHs after sulfate adsorption (Fig. 2(c)), the band at 3,449 cm^{-1} was shifted to 3,502 cm^{-1}, which corroborated the interaction of sulfate anions with the hydroxyl groups on adsorbent. A new peak appeared at 1,109 cm^{-1} can be ascribed to S–O bond [12], indicating that sulfate anions were effectively adsorbed by the adsorbent. The bands at 669 cm^{-1} disappeared and the band at 576 cm^{-1} appeared again, indicating that some interactions occurred in the process of sulfate adsorption by the CLDH adsorbents.

Therefore, according to the adsorption experiments and characterizations analysis, the removal mechanism of sulfate ions by Mg–Fe–CLDHs is presumed mainly by the so-called "memory effect" in which the Mg–Fe–CLDHs with chemical formula of $Mg_{1-x}Fe_xO_{1+x/2}$ can be rehydrated and the anions of sulfate intercalated into the interlayer of LDHs. The possible adsorption process might be explained as the following ways:

$$2Mg_{1-x}Fe_xO_{1+x/2} + (x)SO_4^{2-} + (3+x)H_2O \rightarrow [Mg_{1-x}Fe_x(OH)_2]_2(SO_4)_x \cdot H_2O + 2xOH^-$$

OH^- is produced during the rehydration of Mg–Fe–CLDHs and it is consistent with the above experiments results.

4. Conclusions

In this work, Mg–Fe–CLDHs were developed as adsorbents with much higher uptake capability to remove sulfate in natural water. According to the analysis results of ICP, element analysis, XRD, FT-IR, TG-DSC, BET and SEM, Mg–Fe LDH and Mg–Fe–CLDHs were successfully synthesized. Langmuir adsorption isotherm model provided the best fitting of adsorption isotherms with the experimental data. A maximum capacity of sulfate at equilibrium (q_e = 68 mg/L) with a fixed adsorbent dose of 7.4 g/L was observed at 30˚C after 4-h equilibrium. Adsorption kinetic pattern could be well described by a pseudo-second-order kinetic model. The intraparticle diffusion model shows that adsorption mechanism is complex. The XRD and FT-IR analysis after rehydration shows that Mg–Fe–CLDHs can rehydrate and adsorb sulfate effectively. The adsorption mechanism for sulfate involved surface adsorption, ion exchange interaction and reconstruction of its original layered structure. Among them, reconstruction is the rate-determining step.

Acknowledgments

The authors are grateful for the financial support from Scientific and technological project of Shanxi Province, China Grant number [20120311008-1].

References

[1] WHO (World Health Organization), Guidelines for Drinking-Water Quality, fourth ed., Geneva, World Health Organization, 2011, pp. 227.
[2] G. Madzivire, L.F. Petrik, W.M. Gitari, T.V. Ojumu, G. Balfour, Application of coal fly ash to circumneutral mine waters for the removal of sulphates as gypsum and ettringite, Miner. Eng. 23 (2010) 252–257.
[3] C. Namasivayam, D. Sangeetha, Application of coconut coir pith for the removal of sulfate and other anions from water, Desalination 219 (2008) 1–13.
[4] P. Nurmi, B. Özkaya, K. Sasaki, A.H. Kaksonen, M. Riekkola-Vanhanen, O.H. Tuovinen, J.A. Puhakka, Biooxidation and precipitation for iron and sulfate removal from heap bioleaching effluent streams, Hydrometallurgy 101 (2010) 7–14.
[5] R. Silva, L. Cadorin, J. Rubio, Sulphate ions removal from an aqueous solution: I. Co-precipitation with hydrolysed aluminum-bearing salts, Miner. Eng. 23 (2010) 1220–1226.

[6] H.M. Krieg, S.J. Modise, K. Keizer, H.W.J.P. Neomagus, Salt rejection in nanofiltration for single and binary salt mixtures in view of sulphate removal, Desalination 171 (2005) 205–215.
[7] M. Murugananthan, G.B. Raju, S. Prabhakar, Removal of sulfide, sulfate and sulfite ions by electro coagulation, J. Hazard. Mater. 109 (2004) 37–44.
[8] N.J. Bunce, M. Chartrand, P. Keech, Electrochemical treatment of acidic aqueous ferrous sulfate and copper sulfate as models for acid mine drainage, Water Res. 35 (2001) 4410–4416.
[9] W. Cao, Z. Dang, X.Q. Zhou, X.Y. Yi, P.X. Wu, N.W. Zhu, G.N. Lu, Removal of sulphate from aqueous solution using modified rice straw: Preparation, characterization and adsorption performance, Carbohydr. Polym. 85 (2011) 571–577.
[10] K.H. Goha, T.T. Lima, Z. Dong, Application of layered double hydroxides for removal of oxyanions: A review, Water Res. 42 (2008) 1343–1368.
[11] Z.M. Ni, S.J. Xia, L.G. Wang, F.F. Xing, G.X. Pan, Treatment of methyl orange by calcined layered double hydroxides in aqueous solution: Adsorption property and kinetic studies, J. Colloid Interface Sci. 316 (2007) 284–291.
[12] W. Meng, F. Li, D.G. Evans, X. Duan, Preparation and intercalation chemistry of magnesium–iron(III) layered double hydroxides containing exchangeable interlayer chloride and nitrate ions, Mater. Res. Bull. 39 (2004) 1185–1193.
[13] D. Kang, X. Yu, S. Tong, M. Ge, J. Zuo, C. Cao, W. Song, Performance and mechanism of Mg/Fe layered double hydroxides for fluoride and arsenate removal from aqueous solution, Chem. Eng. J. 228 (2013) 731–740.
[14] Y. Guo, Z. Zhu, Y. Qiu, J. Zhao, Enhanced adsorption of acid brown 14 dye on calcined Mg/Fe layered double hydroxide with memory effect, Chem. Eng. J. 219 (2013) 69–77.
[15] J. Das, B. Sairam Patra, N. Baliarsingh and K.M. Parida, Calcined Mg–Fe–CO_3 LDH as an adsorbent for the removal of selenite, J. Colloid Interface Sci. 316 (2007) 216–223.
[16] Y. Yang, N. Gao, W. Chu, Y. Zhang, Y. Ma, Adsorption of perchlorate from aqueous solution by the calcination product of Mg/(Al–Fe) hydrotalcite-like compounds, J. Hazard. Mater. 209–210 (2012) 318–325.
[17] K.S. Triantafyllidis, E.N. Peleka, V.G. Komvokis, P.P. Mavros, Iron-modified hydrotalcite-like materials as highly efficient phosphate sorbents, J. Colloid Interface Sci. 342 (2010) 427–436.
[18] S. Tezuka, R. Chitrakar, A. Sonoda, K. Ooi, T. Tomida, Studies on selective adsorbents for oxo-anions. Nitrate ion-exchange properties of layered double hydroxides with different metal atoms, Green Chem. 6 (2004) 104–109.
[19] O.P. Ferreira, O.L. Alves, D.X. Gouveia, A.G. Souza Filho, J.A.C. de Paiva and J.M. Filho, Thermal decomposition and structural reconstruction effect on Mg–Fe-based hydrotalcite compounds, J. Solid State Chem. 177 (2004) 3058–3069.
[20] G. Carja, R. Nakamura, T. Aida, H. Niiyama, Textural properties of layered double hydroxides: Effect of magnesium substitution by copper or iron, Microporous Mesoporous Mater. 47 (2001) 275–284.
[21] Y. Guo, Z. Zhu, Y. Qiu, J. Zhao, Adsorption of arsenate on Cu/Mg/Fe/La layered double hydroxide from aqueous solutions, J. Hazard. Mater. 239–240 (2012) 279–288.
[22] S.J. Palmer, R.L. Frost, T. Nguyen, Hydrotalcites and their role in coordination of anions in Bayer liquors: Anion binding in layered double hydroxides, Coord. Chem. Rev. 253 (2009) 250–267.
[23] K.S.W. Sing, D.H. Everett, R.A.W. Haul, L. Moscou, R.A. Pierotti, J. Rouquerol, T. Siemieniewska, Reporting physisorption data for gas/solid systems with special reference to the determination of surface area and porosity, Pure Appl. Chem. 57 (1985) 603–619.
[24] J. Dron, A. Dodi, Comparison of adsorption equilibrium models for the study of CL^-, NO^{3-} and SO_4^{2-} removal from aqueous solutions by an anion exchange resin, J. Hazard. Mater. 190 (2011) 300–307.
[25] A. Halajnia, S. Oustan, N. Najafi, A.R. Khataee, A. Lakzian, Adsorption–desorption characteristics of nitrate, phosphate and sulfate on Mg–Al layered double hydroxide, Appl. Clay Sci. 80–81 (2013) 305–312.
[26] Y. Li, B. Gao, T. Wu, W. Chen, X. Li, B. Wang, Adsorption kinetics for removal of thiocyanate from aqueous solution by calcined hydrotalcite, Colloids Surf. A. 325 (2008) 38–43.
[27] Y.S. Ho, G. McKay, Pseudo-second order model for sorption processes, Process Biochem. 34 (1999) 451–465.
[28] M. Islam, R. Patel, Nitrate sorption by thermally activated Mg/Al chloride hydrotalcite-like compound, J. Hazard. Mater. 169 (2009) 524–531.